# Ultrafast relaxation dynamics of photoexcited carriers in GaAs and related compounds

A. J. Taylor,* D. J. Erskine,† and C. L. Tang

*Materials Science Center, Cornell University, Ithaca, New York 14853*

Received October 10, 1984; accepted November 26, 1984

The femtosecond intraband relaxation of hot carriers in GaAs, $Al_{0.32}Ga_{0.68}As$, and the multiple-quantum-well structure is studied using the equal-pulse optical-correlation technique. An overview of the experimental application of this technique to semiconductors is presented. A detailed theoretical analysis of the coherent-artifact contribution to the transmission-correlation peak in the geometry of parallel copropagating beams and a calculation of the saturable-absorption symmetry coefficients for GaAs are given. The relaxation time of carriers from their initially excited states was measured to be in the range 50–100 fsec for the materials studied. The interpretation of the measured relaxation time in terms of electron and hole response functions is discussed. The relevant scattering processes and rates and the corresponding relaxation times calculated from these rates are given.

## 1. INTRODUCTION

The study of the ultrafast dynamics of hot carriers in semiconductors is important for the understanding of the basic physics of scattering processes in semiconductors and has motivated many recent experimental optical studies.[1–5] Moreover, it is crucial to the design of high-speed electronic devices in which the spatial extent approaches the mean free path of the carriers so that the carrier distribution is no longer thermal. We present here a review of our studies[6–8] of the femtosecond intraband relaxation dynamics of hot carriers in GaAs and related materials using optical techniques. We have measured the initial relaxation time $T_r$ characterizing the isotropic depopulation of carriers from their initially photoexcited levels as a function of photoexcited carrier density in GaAs, $Al_{0.32}Ga_{0.68}As$, and a GaAs/AlGaAs multiple quantum-well (MQW) structure at room temperature.

Although our previous papers have discussed mainly the experimental technique and results, we emphasize here the theoretical foundation of the technique and the interpretation of our measurements. We present in Section 2 a brief overview of the application of the equal-pulse technique[9] to the study of semiconductors. In Section 3, a theoretical background for the experiment is provided: The band structure of GaAs and related materials is described and a detailed analysis of the transmission-correlation peak including the contribution of a coherent artifact is presented. This is the first reported detailed analysis of the coherent artifact contribution in the geometry of copropagating beams and calculation of the saturable-absorption symmetry coefficients for $Al_{1-x}Ga_xAs$. In Section 4, we describe the interpretation of the data, including the determinations of $T_r$ and its relation to the behavior of the conduction and valence carrier distributions. In Section 5, we address the issue of attributing $T_r$ to a specific scattering process by itemizing the relevant scattering mechanisms and then estimating their rates.

## 2. EXPERIMENT

The equal-pulse correlation technique is based on the saturation effect in the transmission of two laser pulses through a thin sample. The two pulses, which are orthogonally polarized, collinearly propagating, and equal in energy, are focused on the sample with an intensity such that saturable absorption occurs. Their combined, time-averaged, transmitted flux is measured as a function of temporal delay $\tau$. This transmitted flux reaches a peak at $\tau = 0$ and reduces to a background value when $\tau$ becomes much greater than the relaxation time of the absorption process and the laser pulse width. We call this peak a transmission correlation peak (TCP). In general, it consists of an incoherent portion ($TCP_i$), whose shape yields information on the relaxation processes that depopulate the photoexcited state, and a coherent artifact (CA), whose shape contains no such information. Figure 1 shows a typical experimental TCP scan for an AlGaAs sample where the time-averaged transmitted flux of both pulses versus $\tau$ is displayed. An autocorrelation (AC) of the laser pulse is also shown.

The equal-pulse correlation technique is particularly useful when studying processes that occur on time scales comparable with or faster than the pulse width (i.e., intraband relaxation) in the presence of much slower processes (such as interband relaxation), since the TCP corresponding to the fast decay process is then clearly revealed as a symmetrical, narrow peak on the flat background, which corresponding to the slow decay. After subtraction of the CA from the TCP, the remaining narrow peak is then proportional to a convolution of the AC and a double-sided exponential with decay time $T_r$ corresponding to the fast process. In contrast, when the conventional pump-probe technique is used,[10] fast processes are obscured by the step in transmission at $\tau = 0$ and by the long decay. A fast decay is revealed mainly through a modification of the rise of the initial step, making it difficult to determine $T_r$ for the fast process.

The experimental arrangement for measuring the TCP is shown in Fig. 2. A passively mode-locked ring laser operating in the colliding-pulse mode produces a train of 90-fsec pulses at 612 nm and at a repetition rate of $10^8$ Hz. The pulse train is divided into two arms of orthogonal polarization and equal power by the half-wave plate and the polarizing beam splitter. After retroreflection from the corner-cube prisms, the two arms are recombined collinearly. The time delay between the

0740-3224/85/040663-11$02.00 

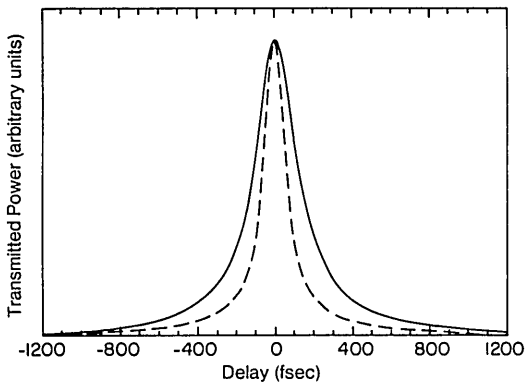


Fig. 1. The solid curve is a TCP for a sample of AlGaAs, and the dashed curve is an AC of the laser pulse.

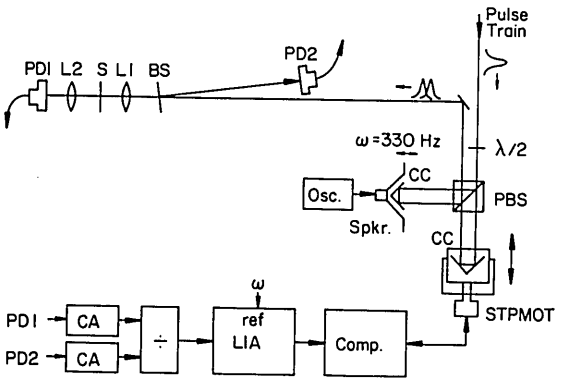


Fig. 2. Optical setup for the equal-pulse correlation technique. PBS, BS, 50% polarizing and 4% ordinary beam splitters, respectively; λ/2, half-wave plate; CC, retroreflecting corner cubes; SPKR, speaker; STPMOT, stepping-motor-driven linear actuator; PD1, PD2, P-I-N photodiodes. L1, L2, 40× and 20× microscope objectives, respectively; S, sample; CA, current amplifier; ÷, dividing circuit; LIA, lock-in amplifier; Comp., computer.

two arms, $\tau$, is determined by the instantaneous positions of the speaker and the linear translator on which the corner cubes are mounted. The recombined pulse train is focused onto the sample by lens L1. The transmitted light is collected by lens L2, and the time-averaged transmitted flux is detected by photodiode PD1. To correct for fluctuations in the laser power during a scan, a portion of the pulse train is reflected by a beam splitter onto PD2. The two photodiodes are connected to current amplifiers, the outputs of which are divided to yield a normalized signal. The resulting signal is digitized and stored by computer for subsequent numerical analysis.

We use a derivative dither technique to improve the signal-to-noise ratio. The speaker corner cube is dithered at a frequency $\omega = 330$ Hz with an excursion of 15 fsec (about 10% of the TCP width). For each value of the average time delay set by the linear translator, the lock-in amplifier detects the component of the signal at $\omega$. A scan is made by recording the amplitude of this component as a function of average delay. Since the dither amplitude is small compared with the width of the TCP, the amplitude of the $\omega$ component is proportional to the derivative of the TCP with respect to $\tau$. After the scan is complete, it is integrated numerically to yield the TCP versus $\tau$, as is shown in Fig. 1. The AC is taken using the same experimental setup and method, with an ordinary beam splitter replacing the polarizing one, a 75-$\mu$m-thick ammonium dihydrogen phosphate (ADP) crystal in place of the sample, and a photomultiplier tube detecting the generated second harmonic light.

Results on three semiconductor samples are reported in this paper: (1) a layer of undoped GaAs 0.3 $\mu$m thick cladded by 0.15-$\mu$m layers of transparent (to 612-nm light) $Al_{0.6}Ga_{0.4}As$, (2) a 0.25-$\mu$m-thick uncladded layer of $Al_{0.32}Ga_{0.68}As$, and (3) a MQW structure consisting of five 15-nm-thick undoped GaAs wells between 70-nm $Al_{0.7}Ga_{0.3}As$ barriers. All the samples were grown by the conventional low-pressure modified chemical-vapor deposition process, and the substrates were removed in a 375-$\mu$m circle by chemical etching.

## 3. THEORY

### A. Band Structure of GaAs and Related Materials

Figure 3 displays a schematic of the band structures of GaAs, revealing the heavy-hole, light-hand, and split-off valence bands as well as portions of the conduction band along a (111) direction in $k$ space. The conduction band has three relevant minima: the central valley or $\Gamma$ valley at $k = 0$, the $L$ valley at $k \sim 10^8$ cm$^{-1}$ in the (111) direction, and the $X$ valley (not shown) at $k \sim 10^8$ cm$^{-1}$ in the (100) direction. Although there are no direct 2.02-eV transitions to the $L$ or $X$ valley, these outer valleys participate in important scattering processes. The three direct transitions for 2.02-eV photons in GaAs are indicated in Fig. 3 by the vertical lines. These transitions originate from the heavy-hole (h), light-hole (l), and split-off (s) valence bands. The density of states in the optically coupled regions (OCR's) for the $h$ and $l$ transitions are nearly equal, whereas the number of levels in the OCR of the split-off band is estimated to be 15% of the total number of levels in all three OCR's.

The band structure of $Al_{0.32}Ga_{0.68}As$ is also displayed in Fig. 3. In AlGaAs the heavy- and light-hole conduction-band OCR's are much closer to the bottom of the central valley than in GaAs (0.17 and 0.10 eV versus 0.51 and 0.45 eV, respectively), which affects the magnitude of some scattering rates. As in GaAs, the densities of states in the OCR for the heavy- and light-hole transitions are roughly equal; however, in AlGaAs there is no 2.02-eV transition from the split-off band owing to the large band gap. Table 1 lists the values of various parameters[11] for the band structures of GaAs and AlGaAs.

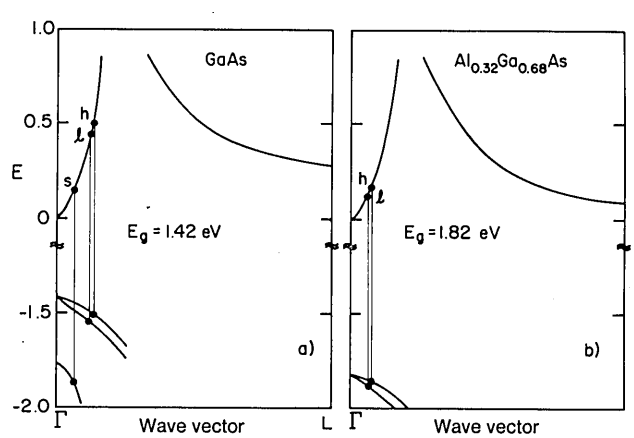


Fig. 3. Band structures of a) GaAs and b) $Al_{0.32}Ga_{0.68}As$, showing the three valence bands and the central and $L$ valleys of the conduction band. h, l, and s mark the levels optically coupled by the allowed transitions for a 2.02-eV photon from the heavy-hole, light-hole, and split-off valence bands, respectively, to the conduction band.

**Table 1. Band-Structure Parameters**[a]

| Parameters | GaAs | AlGaAs |
|---|---|---|
| Mass[b] | | |
| $m_{\Gamma h}$ | 0.5 | 0.6 |
| $m_{\Gamma s}$ | 0.145 | same[e] |
| $m_{\Gamma c}$ | 0.063 | 0.09 |
| $m_L$ | 0.222 | same |
| $m_X$ | 0.58 | same |
| Energy (eV)[c] | | |
| $E_g$ | 1.42 | 1.82 |
| $\Delta_{\Gamma L}$ | 0.29 | 0.09 |
| $\Delta_{\Gamma X}$ | 0.48 | 0.14 |
| Nonparabolicities[d] | | |
| $\alpha_\Gamma$ | 0.62 | same |
| $\alpha_L$ | 0.46 | same |
| $\alpha_X$ | 0.20 | same |

[a] See Ref. 11.

[b] $m_{\Gamma h,\Gamma s,\Gamma c,L,X}$ are the masses in units of the free-electron mass of the carriers in the heavy and split-off valence bands, in the central-valley conduction band, and in the $L$ and $X$ valleys of the conduction band.

[c] $E_g$ is the band gap. $\Delta_{ij}$ are the energy differences between the minima of the various valleys.

[d] $\alpha_i$ is the nonparabolicity of the various valleys defined by Eq. (28).

[e] "Same" means that a value appropriate to $Al_{0.32}Ga_{0.68}As$ could not be found and that the GaAs value was assumed.

### B. Transmission Correlation Peak

To describe the TCP, we use the formalism of Ref. 12, in which the density-matrix equations are iteratively solved for the three-level system consisting of two levels and a resevoir that describes a saturable absorber interacting with an electromagnetic field to calculate the resultant third-order nonlinear polarization. For propagation in the $y$ direction the total incident electric-field envelope has the form

$$\mathbf{E}(t,r) = \exp(iky)\sum_j E_j(t)\hat{e}_j \tag{1}$$

and results in a third-order nonlinear polarization whose envelope is given by

$$\mathbf{P}^{(3)}(t,r) \propto \exp(iky)\sum_{ijkl}\hat{e}_i E_j(t) \times \int_0^\infty dw\, E_k^*(t-w)E_l(t-w)A_{ijkl}(t-\omega). \tag{2}$$

$A_{ijkl}$ is the impulse response of the third-order susceptibility for the combination of electric fields $E_i^* E_j E_k^* E_1$:

$$A_{ijkl}(t) = \{Y_{ij}Y_{kl}[1-\exp(-t/T_0)] + Y_{ijkl}\exp(-t/T_0)\}G(t). \tag{3}$$

$G(t)$ is the impulse response of the population of the photoexcited state. [Note that $T_r$ is the relaxation time describing the initial decay of $G(t)$]. $T_0$ is the orientational diffusion time that characterizes the decay of the photoexcited anisotropy of the material. $Y_{ij}$ and $Y_{ijkl}$ are coefficients, derived from projection integrals of the transition-matrix elements, which describe the symmetry of the saturable-absorption process.

If the excited-state wave functions $\phi_c{}^\gamma$ are $N_2$-fold degenerate wave functions, with $\gamma$ labeling the degeneracy parameter, and the ground-state wave functions $\phi_v{}^\delta$ are $N_1$-fold degenerate, with $\delta$ labeling the degeneracy, then the transition-matrix element $\mathbf{r}_{cv}{}^{\gamma\delta}$ is defined as

$$\mathbf{r}_{cv}{}^{\gamma\delta} = \langle c\gamma|\,\mathbf{r}\,|v\delta\rangle. \tag{4}$$

The $Y$ parameters can then be written in terms of $\mathbf{r}_{cv}{}^{\gamma\delta}$ in the following manner:

$$Y_{ij}Y_{kl} = 9/(32\pi^2 N_1)\sum_{\gamma=1}^{N_2}\sum_{\beta=1}^{N_2}\sum_{\delta=1}^{N_1}\sum_{\alpha=1}^{N_1} \times (\int d\Omega\, \mathbf{r}_{cv}{}^{\gamma\delta *}\cdot\hat{e}_i^*\,\mathbf{r}_{cv}{}^{\gamma\delta}\cdot\hat{e}_j) \times (\int d\Omega[\mathbf{r}_{cv}{}^{\gamma\alpha *}\cdot\hat{e}_k^*\,\mathbf{r}_{cv}{}^{\gamma\alpha}\cdot\hat{e}_l + \mathbf{r}_{cv}{}^{\beta\delta *}\cdot\hat{e}_k^*\,\mathbf{r}_{cv}{}^{\beta\delta}\cdot\hat{e}_l]), \tag{5a}$$

$$Y_{ijkl} = 9/(8\pi^2 N_1)\sum_{\gamma=1}^{N_2}\sum_{\beta=1}^{N_2}\sum_{\delta=1}^{N_1}\sum_{\alpha=1}^{N_1} \times \int d\Omega[(\mathbf{r}_{cv}{}^{\gamma\delta *}\cdot\hat{e}_i^*\,\mathbf{r}_{cv}{}^{\gamma\delta}\cdot\hat{e}_j) \times (\mathbf{r}_{cv}{}^{\gamma\alpha *}\cdot\hat{e}_k^*\,\mathbf{r}_{cv}{}^{\gamma\alpha}\cdot\hat{e}_l + \mathbf{r}_{cv}{}^{\beta\delta *}\cdot\hat{e}_k^*\,\mathbf{r}_{cv}{}^{\beta\delta}\cdot\hat{e}_l)]. \tag{5b}$$

Our definition of the $Y$ parameters differs from that of Ref. 12 since we need to consider the degeneracies that occur in the conduction and valence bands in GaAs. This extension to the degenerate case follows simply from the density-matrix formalism. Note also that we use the matrix elements of $\mathbf{r}$ and not those of its unit vector in the above definitions, since the extension to the degenerate case is then more straightforward; however, the $Y$ parameters are no longer dimensionless.

In the small-signal regime, the induced change in absorption,[13] and hence the induced change in transmitted intensity, $\Delta I$, is given by

$$\Delta I = -\mathrm{Im}[\mathbf{E}^*(t)\cdot\mathbf{P}^{(3)}(t)]. \tag{6}$$

Since the TCP is the time-averaged change in the transmitted light as a function of delay $\tau$ between two input pulses, it is found by combining expressions (2) and (6) that

$$\mathrm{TCP}(\tau) \propto \sum_{ijkl}\int_0^\infty dw A_{ijkl}(w) \times \int_{-\infty}^\infty E_i^*(t)E_j(t)E_k^*(t-w)E_l(t-w)dt. \tag{7}$$

Experimentally, the two input pulses are equal in intensity, collinearly propagating, and orthogonally polarized ($o$). In this case only six terms are nonzero in expression (7):

$$\begin{aligned}\mathrm{TCP}_o(\tau) \propto \int_0^\infty dw \Big\{ & A_{xxzz}(w) \times \int_{-\infty}^\infty dt[E^*(t)E(t)E^*(t-w+\tau)E(t-w+\tau)] \\ & + A_{zzxx}(w)\int_{-\infty}^\infty dt[E^*(t+\tau)E(t+\tau) \times E^*(t-w)E(t-w)] + A_{xzzx}(w) \\ & \times \int_{-\infty}^\infty dt[E^*(t)E(t+\tau)E^*(t-w+\tau)E(t-w)] \\ & + A_{zxxz}(w)\int_{-\infty}^\infty dt[E^*(t+\tau)E(t)E^*(t-w) \times E(t-w+\tau)] + \exp(-2i\omega\tau)A_{xzxz}(w) \\ & \times \int_{-\infty}^\infty dt[E^*(t)E(t+\tau)E^*(t-w)E(t-w+\tau)] \\ & + \exp(2i\omega t)A_{zxzx}(w)\int_{-\infty}^\infty dt[E^*(t+\tau)E(t) \times E^*(t-w+\tau)E(t-w)]\Big\}. \end{aligned} \tag{8}$$

The last two terms in expression (8) oscillate with $\tau$ as $\exp(2i\omega\tau)$ and therefore are seen only if the experiment resolves fringes separated by 1 fsec (or 0.15-$\mu$m steps in a delay line). Although the existence of these fringes has been identified experimentally,[14] our setup is not sensitive to them, since we dither over a ±15-fsec interval at each position of the delay line. If these fringing terms are averaged out to zero by experimental conditions, then expression (8) becomes

$$\mathrm{TCP}_o(\tau) \propto \int_0^\infty dw A_{xxzz}(w)[\mathrm{AC}(\tau - w) + \mathrm{AC}(\tau + w)] + \int_0^\infty dw A_{xzzx}(w)[\zeta(w, \tau) + \zeta(w, -\tau)], \quad (9)$$

where the symmetry properties of the $Y$ parameters[12] have been used. $\mathrm{AC}(\tau)$ is the AC of the pulse intensity envelope, and $\zeta(w, \tau)$ is given by

$$\zeta(w, \tau) = \int_{-\infty}^\infty dt E^*(t)E(t + \tau)E^*(t + \tau - w)E(t - w). \quad (10)$$

An expression for the TCP when the input pulses have parallel polarizations ($p$) is

$$\mathrm{TCP}_p(\tau) \propto \int_0^\infty dw A_{zzzz}(w)[\mathrm{AC}(\tau - w) + \mathrm{AC}(\tau + w)] + \int_0^\infty dw A_{zzzz}(w)[\zeta(w, \tau) + \zeta(w, -\tau)]. \quad (11)$$

[Again fringing terms proportional to $\exp(2i\omega\tau)$ are assumed to have been averaged to zero by the experimental conditions.]

### C. Coherent and Incoherent Contributions to the Transmission-Correlation Peak

The first term in expressions (9) and (11) represents the incoherent contribution $[\mathrm{TCP}_i(\tau)]$ to the saturation process. This is the term that provides information on the relaxation of the populations of the photoexcited state. It is proportional to the convolution of the AC and the response function of the photoexcited state. The second term in expressions (9) and (11) is the CA contribution to the TCP. $\mathrm{CA}(\tau)$ provides no information on the relaxation of the photoexcited state, as it is nonzero only when $\tau$ is less than the coherence time of the pulse. If the relevant relaxation process of the material has a decay constant much longer than the laser pulse width, then the CA will not present a problem, since it will simply appear as a spike at $\tau = 0$. However, for processes that are faster than the pulse width, such as intraband relaxation, the amplitude of the CA at $\tau = 0$ as well as its shape must be determined. The CA can then be subtracted from the total TCP, yielding $\mathrm{TCP}_i$, from which a relaxation time may be extracted.

If the laser pulses are bandwidth limited, then the shape of the CA will be approximately the same as the AC. However, the shape of the CA can be more accurately derived from a measurement of the TCP, in which the sample is a thin jet of an organic dye in solution. The central narrow peak in such dyes as Nile blue in ethylene glycol has been determined to be almost completely (>90%) due to the CA.[8,14] Since the shape of the CA depends mainly on the coherence properties of the pulse and only weakly on material parameters, we can use this CA from organic-dye molecules to approximate the CA for other materials such as semiconductors.

We define the fractional amount of CA (FCA) at $\tau = 0$ for either parallel ($p$) or orthogonally ($o$) polarized input beams as

$$\mathrm{FCA}_{p,o} = \mathrm{CA}(0)_{p,o}/\mathrm{TCP}(0)_{p,o}. \quad (12)$$

An examination of expressions (3), (11), and (12) reveals that $\mathrm{FCA}_p = 1/2$. $\mathrm{FCA}_o$ depends on the $Y$ parameters and on $T_o$. Since $Y_{ij} = 0$ if $i \neq j$, expressions (3), (9), and (10) reveal that, in the orthogonal configuration, the CA is negligible when the absorption properties of the material are polarization independent ($Y_{xzzx} = 0$) or when $T_o$ is much shorter than both the pulse width and the faster energy relaxation process. A simple expression for $\mathrm{FCA}_o$ can be derived when the following assumptions are made: (1) The response function is of the form $G(t) = \exp(-t/T_r)$, (2) $T_o$ and $T_r$ are less than the pulse width, and (3) the electric-field envelope is real and temporally Gaussian:

$$\mathrm{FCA}_o = (T_o/T_r)\, Y_{xzzx}/[(T_o/T_r)(Y_{xzzx} + Y_{xxzz}) + Y_{zz}{}^2]. \quad (13)$$

Therefore to estimate $\mathrm{FCA}_o$ one needs the $Y$ parameters that can be calculated theoretically and the ratio $T_o/T_r$ that can be found from a measurement of the ratio $R$ defined as

$$R = \mathrm{TCP}(0)_p/\mathrm{TCP}(0)_o. \quad (14)$$

Using the approximations listed above, $R$ becomes

$$R = 2[Y_{zz}{}^2 + Y_{zzzz}(T_o/T_r)]/ \times [Y_{zz}{}^2 + (Y_{xzzx} + Y_{xxzz})(T_o/T_r)], \quad (15)$$

which we can solve for $T_o/T_r$ in terms of $R$ as

$$T_o/T_r = Y_{zz}{}^2(2 - R)/[R(Y_{xzzx} + Y_{xxzz}) - 2Y_{zzzz}]. \quad (16)$$

Using Eqs. (13) and (16), the calculated values of the $Y$ parameters, and the experimentally determined value of $R$, the amplitude of the CA contribution to the TCP can be determined. Assuming that the shape of the CA can be approximated by the dye TCP, the CA can then be subtracted from the total TCP. The remaining $\mathrm{TCP}_i$ can then be analyzed to determine the relaxation times of the system. Independent of the above assumptions, we note that when $T_o = 0$, $R = 2$ and no CA is present. Conversely, when $T_o = \infty$, $R = 2Y_{zzzz}/(Y_{xzzx} + Y_{xxzz})$ and there is a maximum $\mathrm{FCA}_o$ of $Y_{xzzx}/(Y_{xzzx} + Y_{xxzz})$.

### D. *Y* Parameters

To calculate the $Y$ parameters using Eqs. (5), we need the transition-matrix elements and hence the wave functions. Kane[15] derives the wave functions for direct-gap semiconductors with a zinc-blende structure by using a $\mathbf{k} \cdot \mathbf{p}$ perturbation approach and taking into account the spin–orbit interaction. There are six doubly degenerate valence-band states, corresponding to the heavy-hole ($h$), light hole ($l$), and split-off ($s$) valence bands, and two degenerate conduction ($c$) band states. In the body-fixed coordinate system, where $\mathbf{k}$ is in the $z$ direction, these wave functions have the following form:

**Table 2. Relevant Parameters for the 2.02-eV Transitions in GaAs and $Al_{0.32}Ga_{0.68}As$**

| Transitions | Parameters | | | | | |
|---|---|---|---|---|---|---|
| | $k$ (cm$^{-1}$) | $E_c$ (eV) | $E_v$ (eV) | $\Delta$ (eV) | $E_g$ (eV) | $P$ (eV/cm) |
| GaAs | | | | 0.34 | 1.42 | $9.58 \times 10^{-8}$ |
| Heavy hole | $1.06 \times 10^7$ | 1.93 | −0.086 | | | |
| Light hole | $0.97 \times 10^7$ | 1.87 | −0.152 | | | |
| Split off | $0.52 \times 10^7$ | 1.57 | −0.45 | | | |
| AlGaAs | | | | 0.31 | 1.82 | $9.00 \times 10^{-8}$ |
| Heavy hole | $0.66 \times 10^7$ | 1.99 | −0.028 | | | |
| Light hole | $0.51 \times 10^7$ | 1.92 | −0.080 | | | |

**Table 3. Wave-Function Coefficients for the Possible 2.02-eV Transitions in GaAs and $Al_{0.32}Ga_{0.68}As$**

| Transitions | Bands | Coefficients | | |
|---|---|---|---|---|
| | | $a_i$ | $b_i$ | $c_i$ |
| GaAs | | | | |
| Heavy hole | Conduction | 0.91 | 0.032 | 0.42 |
| Light hole | Valence | 0.13 | −0.96 | −0.23 |
| Light hole | Conduction | 0.91 | 0.032 | 0.40 |
| Split off | Valence | −0.22 | −0.55 | 0.80 |
| Split off | Conduction | 0.97 | 0.024 | 0.27 |
| AlGaAs | | | | |
| Heavy hole | Conduction | 0.97 | 0.017 | 0.25 |
| Light hole | Valence | 0.15 | −0.78 | −0.61 |
| Light hole | Conduction | 0.97 | 0.016 | 0.24 |

**Table 4. Transition-Matrix Element $\mathbf{r}_{cv}{}^{\gamma\delta}$ for the Various Valence- to Conduction-Band Transitions for the Direct-Gap Semiconductors Described by the Wave Functions of Eqs. (17) and (18)[a]**

| Matrix Elements | | Transitions | |
|---|---|---|---|
| | | $\gamma = 1/2$ | $\gamma = -1/2$ |
| $\mathbf{r}_{ch}{}^{\gamma\delta'}$ | $\delta = 3/2$ | $ia_c r(\hat{x} + i\hat{y})/6^{1/2}$ | 0 |
| | $\delta = -3/2$ | 0 | $ia_c r(\hat{x} - i\hat{y})/6^{1/2}$ |
| $\mathbf{r}_{cl}{}^{\gamma\delta'}$ | $\delta = 1/2$ | $-i\rho r\hat{z}/3^{1/2}$ | $-i\eta r(\hat{x} + i\hat{y})/6^{1/2}$ |
| | $\delta = -1/2$ | $i\eta r(\hat{x} - i\hat{y})/6^{1/2}$ | $-i\rho r\hat{z}/3^{1/2}$ |
| $\mathbf{r}_{cs}{}^{\gamma\delta'} = \mathbf{r}_{cl}{}^{\gamma\delta'}$ | | | |

[a] $r$ is the reduced matrix element for the transitions. $\rho$ and $\eta$ are derived from the coefficients $a_i$, $b_i$, and $c_i$ by $\rho = a_c c_v - a_v c_c$ and $\eta = a_c b_v - a_v b_c$. $l$ refers to the light-hole transition, $s$ to the split-off transition, and $h$ to the heavy-hole transition. $\mathbf{k}$ is assumed to be in the $z$ direction.

**Table 5. $Y$ Parameters for Direct Band-Gap Semiconductors Described by the Wave Functions of Eqs. (17) and (18)[a]**

| $Y$ Parameter | Transitions | |
|---|---|---|
| | Heavy Hole | Light Hole or Split Off |
| $Y_{zz}$ | $a_c{}^2\|r\|^2/3$ | $(\rho^2 + \eta^2)\|r\|^2/3$ |
| $Y_{zzzz}$ | $2a_c{}^4\|r\|^4/15$ | $(3\rho^4 + 2\eta^4 + 2\rho^2\eta^2)\|r\|^4/15$ |
| $Y_{xxzz}$ | $a_c{}^4\|r\|^4/10$ | $(2\rho^4 + 3\eta^4 + 8\rho^2\eta^2)\|r\|^4/30$ |
| $Y_{xzzx}$ | $a_c{}^4\|r\|^4/10$ | $(2\rho^4 + 3\eta^4 - 2\rho^2\eta^2)\|r\|^4/30$ |

[a] $r$ is the reduced matrix element for the transitions. $\rho$ and $\eta$ are derived from the coefficients $a_i$, $b_i$, and $c_i$ by $\rho = a_c c_v - a_v c_c$ and $\eta = a_c b_v - a_v b_c$, where $v = 1$ for the light-hole transition and $v = s$ for the split-off transition.

**Table 6. $Y$ Parameters[a] for the Possible 2.02-eV Transitions in GaAs and $Al_{0.32}Ga_{0.68}As$**

| Transitions | $Y$ Parameters | | | |
|---|---|---|---|---|
| | $Y_{zz}$ | $Y_{zzzz}$ | $Y_{xxzz}$ | $Y_{xzzx}$ |
| GaAs | | | | |
| Heavy hole | 0.28 | 0.091 | 0.069 | 0.069 |
| Light hole | 0.28 | 0.087 | 0.074 | 0.056 |
| Split off | 0.33 | 0.135 | 0.093 | 0.027 |
| Total | 0.29 | 0.092 | 0.073 | 0.060 |
| AlGaAs | | | | |
| Heavy hole | 0.31 | 0.118 | 0.089 | 0.089 |
| Light hole | 0.32 | 0.105 | 0.104 | 0.029 |
| Total | 0.31 | 0.112 | 0.096 | 0.059 |

[a] The total $Y$ parameter for the 2.02-eV transition can be found by averaging each $Y$ parameter over the possible transitions, weighting each one by the density of states squared. $Y_{zz}$ is given in units of $|r|^2$, and $Y_{zzzz}$, $Y_{xxzz}$, and $Y_{xzzx}$ are given in units of $|r|^4$, where $r$ is the reduced matrix element for the transitions.

$$\phi_h{}^{3/2} = [(X + iY)\uparrow]/2^{1/2}, \tag{17a}$$

$$\phi_h{}^{-3/2} = [(X - iY)\downarrow]/2^{1/2}, \tag{17b}$$

$$\phi_i{}^{1/2} = a_i[iS\uparrow] + b_i[-(X + iY)\downarrow]/2^{1/2} + c_i[Z\uparrow], \tag{17b'}$$

$$\phi_i{}^{-1/2} = a_i[iS\downarrow] + b_i[(X - iY)\uparrow]/2^{1/2} + c_i[Z\downarrow]. \tag{17b'}$$

The indices $\pm 3/2$ and $\pm 1/2$ refer to $M_J$ at $k = 0$, and the index $i$ refers to the $l$, $s$, or $c$ band. $a_i$, $b_i$, and $c_i$ are real coefficients, given by

$$a_i = kP(E'_i + 2/3\Delta)/N, \tag{18a}$$

$$b_i = 2^{1/2}\Delta(E'_i - E_G)/3N, \tag{18b}$$

$$c_i = (E'_i - E_G)(E'_i - 2\Delta/3)/N, \tag{18c}$$

where $N$ is the normalization factor, $E_G$ is the gap energy, $\Delta$ is the spin–orbit splitting, and $E'_i$ is the energy of the state, given by $E_i - \hbar^2k^2/2m$. The symbols $\uparrow$ and $\downarrow$ refer to spin quantum numbers of $\pm 1/2$. The function $S$ has the symmetry properties of the atomic $s$ functions under the operations of the tetrahedral group, while $X$, $Y$, and $Z$ have the symmetry properties of the atomic $p$ functions $x$, $y$, and $z$ under that group. In Table 2 we present the relevant parameters for the 2.02-eV transitions in GaAs and AlGaAs, and in Table 3 we present the wave-function coefficients $a_i$, $b_i$, and $c_i$.

The matrix elements $\mathbf{r}_{cv}{}^{\gamma\delta'}$ for all transitions from the valence band to the conduction band in the body-fixed coordinate system, where $\mathbf{k}$ is in the $z$ direction, are tabulated in Table 4. The laboratory-fixed coordinate system (defined by the $\mathbf{E}$ field) is specified with respect to the body-fixed frame by the usual Euler angles[16] $\alpha$ and $\beta$. ($\gamma$ can be set equal to zero since in the body-fixed frame only the $z$ direction is relevant.) The new matrix elements in this frame, $\mathbf{r}_{cv}{}^{\gamma\delta}$, can be

found from a rotation:

$$\mathbf{r}_{cv}{}^{\gamma\delta} = M\mathbf{r}_{cv}{}^{\gamma\delta'}, \tag{19}$$

where $M$ is a rotation matrix[16] of the form

$$M = \begin{pmatrix} \cos\beta\cos\alpha & -\sin\alpha & \sin\beta\cos\alpha \\ \cos\beta\sin\alpha & \cos\alpha & \sin\beta\sin\alpha \\ -\sin\beta & 0 & \cos\beta \end{pmatrix}. \tag{20}$$

Using Eqs. (5) and (20) and the matrix elements of Table 4, the calculation of the $Y$ parameters is straightforward but tedious. The resulting expressions are tabulated in Table 5 for the three possible transitions.

The calculated values of the $Y$ parameters for the 2.02-eV transition in GaAs and AlGaAs are presented in Table 6. Total $Y$ parameters for the 2.02-eV transition can be found by averaging each $Y$ parameter over the possible transitions and weighting each transition by the density of states squared. These values are also displayed in Table 6.

## 4. INTERPRETATION OF DATA

### A. Determination of Relaxation Times

From the values of the total $Y$ parameters for the 2.02-eV transition, we note that if $T_o = \infty$, then $R = 1.38$ (1.45), resulting in a maximum FCA of 45% (38%) in GaAs (AlGaAs). Experimentally, in both GaAs and AlGaAs we measure $R = 1.75$, which implies [Eqs. (13) and (16)] that $T_o/T_r = 0.43$ in GaAs and $T_o/T_r = 0.51$ in AlGaAs and that FCA = 17% for both materials. When this CA contribution is subtracted from the total TCP, the remaining $\text{TCP}_i$ for the fast process is approximately 30% wider than the corresponding total TCP.

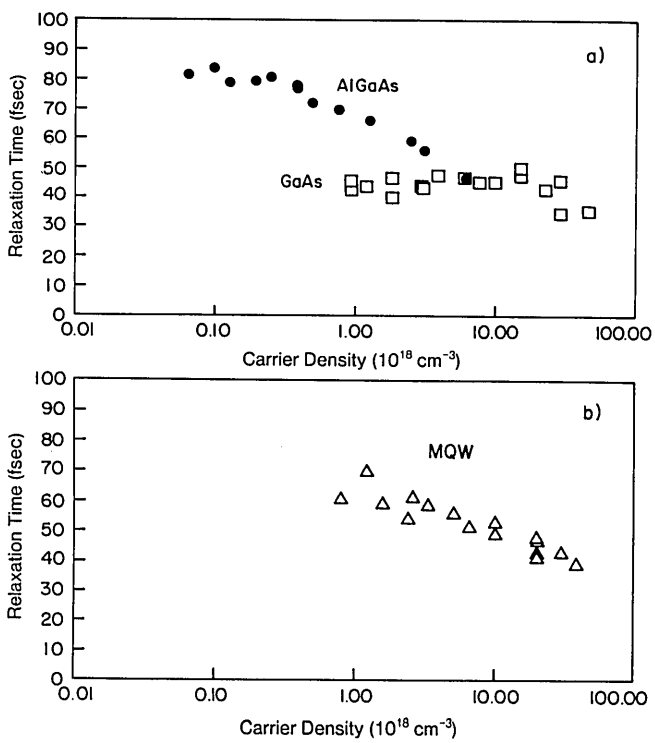


Fig. 4. Relaxation time $T_r$ versus photogenerated carrier density for a) GaAs and AlGaAs and b) MQW.

The values for $T_r$ are determined by deconvolving the measured laser pulse AC from the measured $\text{TCP}_i$. These values for $T_r$ are plotted as a function of photoexcited carrier density $n$ for GaAs, AlGaAs, and the MQW in Fig. 4. At low powers, where carrier–carrier scattering is not expected to be important, $T_r$ is determined by phonon-scattering rates. Thus these data indicate that the phonon rates are greater for GaAs than for AlGaAs. As the input power increases, we expect the carrier-density-dependent scattering rate to grow in importance and compete with the existing photon rates. This is consistent with the downward slope of the curve for AlGaAs. For GaAs, the low-power scattering rate is already large, and the effect of the carrier-density-dependent rate is not seen in the power range studied.

### B. Relation of $T_r$ to Carrier Relaxation Times

Since $T_r$ characterizes the initial portion of the decay of the response function, we must first examine its relation to the carrier relaxation times before interpreting the measured values of $T_r$ in terms of the various scattering processes. We need to determine whether $T_r$ characterizes the behavior of the electron or the hole distributions (or a combination of both). In general, the impulse response function $G(t)$ of the saturable-absorption process is due to both electrons occupying the OCR of the conduction band and holes occupying the OCR of the valence band. Thus $G(t)$ is a weighted sum of both the separate response functions for electrons and holes [$G_e(t)$ and $G_h(t)$, respectively]:

$$G(t) = aG_e(t) + (1-a)G_h(t), \qquad 0 \le a \le 1. \tag{21}$$

The weighting factor $a$ is linked to the number of levels $M_v$ and $M_c$ in the valence- and conduction-band OCR's, respectively. Let the number of filled and vacant levels in the valence-band OCR be $n_v$ and $p_v$, such that $n_v + p_v = M_v$, and those for the conduction-band OCR be $n_c$ and $p_c$, such that $n_c + p_c = M_c$. Then the net change in the number of photons transmitted through a thin layer of material is proportional to $n_v p_c - n_c p_v = M_c M_v - (M_v n_c + M_c p_v)$. Thus if $G_e$ and $G_h$ describe the decay of $n_c$ and $p_v$, then the response function for the saturable absorption is

$$G(t) \propto M_v G_e(t) + M_c G_h(t), \tag{22}$$

and therefore $a = M_v/(M_c + M_v)$.

$M_c$ and $M_v$ are determined by the widths of the OCR's in the conduction and valence bands, respectively. In the case in which the photon bandwidth is large compared with the material linewidth, conservation of momentum ensures that $M_c = M_v$. In the case in which the material linewidth is comparable with or larger than the photon bandwidth, the widths (in energy) of the OCR's in the conduction and valence bands are comparable. If the valence-band effective mass is much larger than the conduction-band effective mass, then $M_v$ can be larger than $M_c$. In this case, $1 > a > \frac{1}{2}$, so that $G(t)$ (and hence $T_r$) describes the response of the electrons more than the response of the holes.

In general, $G(t)$ may be attributed to either $G_e(t)$ or $G_h(t)$ because of different decay behavior of the two response functions. Given that $T_r$ describes the initial decay of $G(t)$ on a time scale of the order of or faster than the pulse width, then if $G_e(t)$ [$G_h(t)$] decays in a time comparable with the pulse width, the measured TCP will emphasize the convolu-

tion of $G_e(t)$ $[G_h(t)]$, if the decay of $G_h(t)$ $[G_e(t)]$ is either very much faster or very much slower than $G_e(t)$ $[G_h(t)]$.

There are two reasons why the decay behavior of $G_e$ and that of $G_h$ may differ. First, $G_e(t)$ and $G_h(t)$ may decay at different rates because the scattering processes, which in part determine the decay behavior, may be different for the conduction and valence bands. This can be checked by simply evaluating the rates of all the relevant scattering processes. Second, $G_e(t)$ and $G_h(t)$ may be affected to different degrees by a band-filling process. (The partial saturation of the OCR owing to carriers in the OCR after relaxation of the initially photoexcited nonequilibrium distribution is termed band filling.) The effect of band filling is to raise the asymptotic level that $G_h(t)$ and $G_e(t)$ approach, so that the influence of the initial decay, corresponding to $T_r$, is reduced in $G_h$ or $G_e$. If the photon bandwidth is much larger than the material bandwidth, then the degree of band filling for the electron and hole distributions will be equal, and this effect will not be relevant. If not, the degree of band filling will be larger in the valence band than in the conduction band, if the effective mass of the holes is much greater than that of the electrons, thus reducing the effective contribution of $G_h$ to the initial decay time $T_r$.

## 5. SCATTERING PROCESSES

The scattering processes that are relevant to calculating the time evolution of the carrier distribution on a subpicosecond time scale can be grouped into two classes: processes in which the basic scattering rate is independent of carrier density, such as carrier–phonon scattering, and processes in which the rate is dependent on carrier density, such as carrier–carrier scattering. We shall first discuss the relevant carrier-density-independent processes, which consist of polar optical phonon (POP) scattering, acoustic phonon scattering (ACS), random potential alloy scattering (ALLOY), and intervalley (IV) phonon scattering. The estimated scattering rates of these processes, calculated from the material parameters given in Table 7, are summarized in Table 8 and are used to calculate a value for $T_r$. This value is compared with the measured value of $T_r$ at low carrier densities, where carrier-density-dependent processes are expected to be less important. Finally, the carrier-density-dependent processes are discussed and their rates are estimated.

**Table 7. Parameters[a] Used in the Calculation of Scattering Rates**

| | |
|---|---|
| Dielectric Constants | $\epsilon_\infty = 10.88$<br>$\epsilon_0 = 12.85$ |
| Central-valley and IV phonon energies | $\hbar\omega_{op} = 0.036$ eV<br>$\hbar\omega_{ij} = 0.8\hbar\omega_{op}$ eV |
| Mass density | $\rho = 5.37$ gm/cm$^3$ |
| Speed of sound | $v_L = 5.22 \times 10^5$ cm/sec |
| Deformation potentials | $D_{acs} = 7$ eV<br>$D_{\Gamma L} = 1 \times 10^9$ eV/cm<br>$D_{\Gamma X} = 1 \times 10^9$ eV/cm |
| Number of equivalent valleys | $Z_l = 4$<br>$Z_X = 3$ |

[a] See Refs. 11 and 20.

### A. Carrier-Density-Independent Processes

The most important intravalley phonon scattering process is POP scattering. Since the energy of an optical phonon ($\hbar\omega_{op} = 0.036$ eV) is relatively independent of its wave vector, the scattered electron loses or gains energy in units of $\hbar\omega_{op}$. In the POP interaction, the displacement of the lattice by the vibration of the optical phonon can cause an induced polarization. This happens only in polar materials, such as $Al_xGa_{1-x}As$, in which the optical mode of the phonon directly changes the separation between the gallium and arsenic atoms. Since these atoms do not carry equivalent charges, a polarization is developed, which in turn interacts strongly with the charged carrier.

The expressions for the scattering rates for absorption of a POP, $R_{POP}{}^+$, and for emission of a phonon, $R_{POP}{}^-$, which include the effects of nonparabolicity of the conduction band but neglect screening, have been derived by Fawcett *et al.*[17]:

$$R_{POP} = e\zeta(2m\gamma)^{1/2}(1 + 2\alpha E')F_o(E, E') \times \begin{cases} N(\omega_{op}) & \text{absorption} \\ N(\omega_{op}) + 1 & \text{emission} \end{cases}, \tag{23}$$

where

$$F_o(E, E') = (1/C)\left[A \ln\frac{|\gamma^{1/2}(E) + \gamma^{1/2}(E')|}{|\gamma^{1/2}(E) - \gamma^{1/2}(E')|} + B\right], \tag{24}$$

$$A = \{2(1 + \alpha E)(1 + \alpha E') + \alpha[\gamma(E) + \gamma(E')]\}^2, \tag{25}$$

$$B = -2\alpha\gamma^{1/2}(E)\gamma(E')\{4(1 + \alpha E)(1 + \alpha E') + \alpha[\gamma(E) + \gamma(E')]\}, \tag{26}$$

$$C = 4(1 + \alpha E)(1 + \alpha E')(1 + 2\alpha E)(1 + 2\alpha E'), \tag{27}$$

$$\gamma(E) = \hbar^2k^2/2m = E(1 + \alpha E), \tag{28}$$

$$E' = \begin{cases} E + \hbar\omega_{op} & \text{for absorption} \\ E - \hbar\omega_{op} & \text{for emission} \end{cases}, \tag{29}$$

$$e\zeta = me^2\omega_{op}(\epsilon_\infty{}^{-1} - \epsilon_o{}^{-1})/\hbar^2, \tag{30}$$

$$N(\omega_{op}) = [\exp(\hbar\omega_{op}/k_BT) - 1]^{-1}. \tag{31}$$

The nonparabolicity coefficient of the valleys ($\alpha$) is defined by Eq. (28). $E$ is the carrier energy measured from the bottom of the valley, and $e\zeta$ is an effective electric field that determines the carrier coupling to the polar modes. $N(\omega_{op})$ is the occupation probability for a phonon having an energy $\hbar\omega_{op}$ and is found from the Bose–Einstein formula. $T$ is the lattice temperature, which is assumed to be 300 K. (Parameters used for calculating scattering rates can be found in Table 7.)

The expression for $R_{POP}{}^{+,-}$ is plotted in Fig. 5 for the parameters of GaAs in the central valley of the conduction band. Note that the rates are independent of carrier energy for energies greater than several optical phonons from the valley floor. The calculated POP scattering rates for the heavy- and light-hole OCR in the conduction and valence bands of GaAs and $Al_{0.32}Ga_{0.68}As$ at 300 K are summarized in Table 8. Finally, note that the POP rates for holes are larger than those for electrons because the magnitude of the rate goes as $m^{1/2}$.

The other intravalley phonon-scattering process is scattering by acoustic phonons. Unlike the optical phonon, the

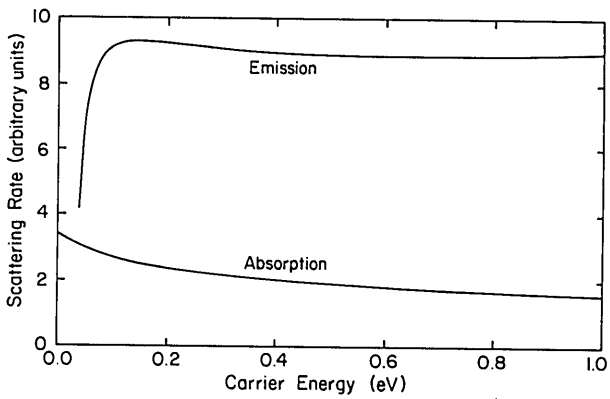


Fig. 5. Scattering rates for emission and absorption of POP's as a function of energy for the conduction band of GaAs. This includes the effects of nonparabolic valleys but neglects screening.

**Table 8. Calculated Scattering Rates[a] from the Heavy and Light OCR**

| Type of Scattering | Scattering Rates | | | |
|---|---|---|---|---|
| | Electron OCR | | Hole OCR | |
| | Heavy | Light | Heavy | Light |
| GaAs | | | | |
| $R_{POP}{}^{+}$ | 1.7 | 1.7 | 5.5 | 5.5 |
| $R_{POP}{}^{-}$ | 6.4 | 6.4 | 18.5 | 18.5 |
| $R_{ACS}$ | 0.6 | 0.6 | 4.7 | 6.2 |
| $R_{ALLOY}$ | 0 | 0 | 0 | 0 |
| $R_{IV}$ | 25(12) | 19(0) | 0 | 0 |
| AlGaAs | | | | |
| $R_{POP}{}^{+}$ | 2.2 | 2.2 | 6.8 | 6.4 |
| $R_{POP}{}^{-}$ | 7.9 | 7.9 | 0 | 19.8 |
| $R_{ACS}$ | 0.5 | 0.4 | 3.5 | 6.3 |
| $R_{ALLOY}$ | 1.0 | 1.0 | 0.4 | 0.4 |
| $R_{IV}$ | 15(9) | 9(0)[f] | 0 | 0 |

[a] Rates are in units of $10^{12}$ sec$^{-1}$. $R_{POP}{}^{+,-}$ is polar optical scattering for absorption (+) and emission (−). $R_{ACS}$ is acoustic and includes emission and absorption of a phonon, $R_{ALLOY}$ is random potential alloy scattering. Note that the latter two rates do not affect the carriers energy but only its momentum; thus they affect only $T_o$ rather than $T_r$. $R_{IV}$ is $\Gamma \rightarrow L$ IV deformation-potential scattering by emission and absorption of a phonon using a deformation potential of $1 \times 10^9$ eV/cm. The values in parentheses are the $\Gamma \rightarrow X$ rates.

energy of the acoustic phonon is small, making the ACS process approximately elastic in nature. However, the momenta of these phonons can be compared with the momenta of the carriers, so that significant changes in carrier momenta can occur. Fawcett *et al.*[17] give the total scattering rate (absorption and emission) assuming parabolic bands as

$$R_{ACS} = 2^{1/2} D_{ACS}{}^2 k_B T E^{1/2} m^{3/2} / (\pi \hbar^4 \rho v_L{}^2), \quad (32)$$

where $\rho$ is the mass density of the material, $v_L$ is the speed of sound, and $D_{ACS}$ is a deformation potential. Generally, the acoustic rate is significantly large only where the effective mass is large, such as for holes. In comparison with the other scattering processes, it is not a significantly large rate for the electron.

Another scattering process, also elastic in nature, is ALLOY. This is only appropriate for the sample of $Al_{0.32}Ga_{0.68}As$ in which inhomogeneities in its composition occur that are due to random fluctuations of the concentrations of aluminum, gallium, and arsenic atoms. These inhomogeneities can act as scattering centers analogous to impurity scattering centers. Random potential scattering is discussed by Hauser *et al.*[19] and Littlejohn *et al.*,[19] where the scattering rate for a general alloy $A_xB_{1-x}C$ is given as

$$R_{ALLOY} = (3\pi m^{3/2}/8\hbar^4 2^{1/2}) x(1-x) \times \gamma(E)(1+2\alpha E)\Omega |\Delta U|^2 S, \quad (33)$$

where $x$ is the mole fraction of element $A$, $\Omega = a^3/4$ is the primitive cell volume, and $a$ is the lattice constant. $S$ is a parameter between 0 and 1 that describes the randomness of the alloy. $S = 0$ would describe a perfectly ordered superlattice, and $S = 1$ a completely random alloy. $\Delta U$ is the scattering potential. $\Delta U$ is taken to be either the difference in energy band gaps between the binary constituents or the difference in electron affinities between the binary constituents. If we take the difference in energy band gaps and attribute 85% to an electron-potential step, as it is usually done in GaAs/AlGaAs heterojunctions, the value for $\Delta U$ is 0.37 for electrons and 0.065 eV for holes. The calculated values for $R_{ALLOY}$, based on these values for $\Delta U$, are given in Table 8.

Both ALLOY and ACS will not significantly affect the value of $T_r$, since these processes do not change the carrier energy enough to remove it from the OCR. To the extent that the OCR is a spherical shell, scattering processes that change only the carrier's momentum will not remove that carrier from the OCR. (The band structure of GaAs is actually slightly nonspherical, so the OCR is slightly fluted. This is expected to have only a minor effect on the scattering rates.) However, these elastic scattering processes are important in determining the orientational relaxation time $T_o$.

In the IV phonon-scattering process an electron scatters from the central valley to one of the outer valleys either by absorption or by emission of a phonon. This process is therefore permitted only when the initial energy of the electron is greater than one optical phonon below the outer-valley minimum. For the $L$ valley in GaAs this energy is greater than 0.3 eV, and in AlGaAs it is greater than 0.1 eV. Because the phonon involved here has a wave vector that is an appreciable fraction of the Brillouin zone, the energy of the optical phonon involved is slightly less than its energy at the zone center ($0.8\hbar\omega_{op}$). This is the most important process in the decay of the electron impulse response. Since there are no outer valleys in the valence band, holes do not participate in IV scattering processes.

Fawcett *et al.*[17] give the IV absorption and emission scattering rates for nonparabolic valleys as

$$R_{IV} = \frac{Z_j m_j{}^{3/2} D_{ij}}{2^{1/2}\pi\rho\omega_{ij}\hbar^2} E_j{}^{1/2} G(E_i, E_j) \times \begin{cases} N(\omega_{op}) & \text{absorption} \\ N(\omega_{op}) + 1 & \text{emission} \end{cases}, \quad (34)$$

where $E_i$ is the initial electron energy measured from the initial ($i$th) valley floor. $E_j$ is the final electron energy measured from the final ($j$th) valley floor, give or take the IV phonon energy $\hbar\omega_{ij}$:

$$E_j = E_i - \Delta_{ij} \pm \hbar\omega_{ij}, \quad (35)$$

where $\Delta_{ij}$ is the energy difference between the floors of the initial and final valleys. $Z_j$ and $m_j$ are the number of equivalent final valleys and the effective mass of the carrier in the final valley. The function $G(E_i, E_j)$ involves the nonparabolicities and is of the order of unity:

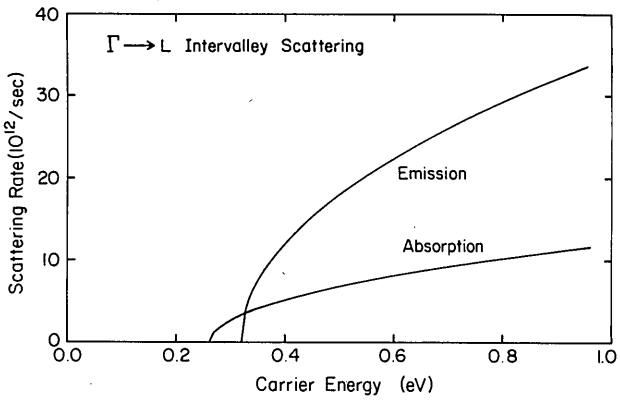


Fig. 6. Scattering rates for emission and absorption of IV phonons, $\Gamma \rightarrow L$, as a function of initial electron energy above the central valley.

$$G(E_i, E_j) = (1 + \alpha_i E_i)(1 + \alpha_i E_i)/[(1 + 2\alpha_i E_i)(1 + 2\alpha_j E_j)]. \quad (36)$$

$D_{ij}$ is the deformation potential specific to the pair of initial and final valleys. We use the value of $D_{ij}$ given by Littlejohn *et al.*[20] Note that this parameter is difficult to determine accurately.

A plot of these rates versus carrier energy for scattering between the central and the $L$ valleys is given in Fig. 6. The energy dependence of the curves is given chiefly by the density of states, which varies as $E^{0.5}$. The values of the $\Gamma \rightarrow L$ and $\Gamma \rightarrow X$ IV rates for the heavy and the light OCR's are tabulated in Table 8 for GaAs and $Al_{0.32}Ga_{0.68}As$ at 300 K. The $\Gamma \rightarrow X$ rates are enclosed in parentheses. The IV scattering rates from the OCR are larger in GaAs than $Al_{0.32}Ga_{0.68}As$ because the OCR's are higher above the bottom of the $L$ valley in GaAs. Although both the light and the heavy OCR's are above the $L$ valley, only the heavy OCR is above the $X$ valley, so the light OCR does not participate in $\Gamma \rightarrow X$ scattering. Since the position of the $X$ valley is not known with great accuracy, it is possible that the $\Gamma \rightarrow X$ rate is different from that given here.

Table 8 summarizes the results of all four scattering processes considered for the heavy and the light OCR's. Clearly, the IV process dominates the scattering in the conduction band. In the valence band where there is no IV scattering, POP scattering is the most significant, but it is not so large as the IV rates for the conduction band. Thus the scattering rate for electrons is calculated to be faster than that for holes, owing to the fast IV rates.

Based on the scattering rates given in Table 8 (for IV scattering to the $L$ valley only), the initially excited electron and hole populations should decay with time constants of 30 and 60 fsec, respectively, in GaAs and 40 and 150 fsec, respectively, in AlGaAs. Because of the considerations discussed earlier, we expect $T_r$ to correspond mainly to the decay of the electron population. This yields calculated decay times of 30 fsec in GaAs and 40 fsec in AlGaAs. The use of only the electron response to determine $T_r$ represents the limit $a = 1$ in Eq. (21) that yields a lower bound for $T_r$. An upper bound for $T_r$ can be found by assuming that the electron and hole populations contribute equally to the response [$a = 0.5$ in Eq. (21)]. In this case, our calculated values for $T_r$ are 40 fsec in GaAs and 80 fsec in AlGaAs. The measured values, at low carrier density, of 45 and 80 fsec are in good agreement with these calculated estimates.

### B. Carrier-Density-Dependent Processes

The values for $T_r$ calculated from carrier–phonon-scattering processes agree well with the measured value of $T_r$ at extreme low carrier densities. However, the variation of the measured data with increasing photoexcited carrier density (Fig. 4) shows that there are carrier-density-dependent processes contributing to $T_r$ that have not yet been taken into account. The relevant carrier-density-dependent processes are the effect of screening on the carrier–phonon scattering rate and carrier–carrier scattering. The latter process manifests different behavior at different carrier densities. At high carrier densities, the collective oscillation of the plasma interactions occur. Free carrier scattering occurs at low carrier densities. Free carrier scattering in turn can be classified as either unlike-particle collisions (electron–hole) or identical-particle collisions (electron–electron, hole–hole).

In general, calculating the effect of these carrier-density-dependent processes on $T_r$ is difficult. Although carrier-density-independent rates permit the determination of the time dependence of the carrier population in the OCR by means of the response or Green's function $G(t)$ (as was assumed to exist in the analyses of the TCP presented in Section 3), for carrier-density-dependent rates, the corresponding rate equations become nonlinear, rendering a response-function approach to the determination of the TCP shape inadequate. As an approximation, a response function is assumed to exist even for carrier-density-dependent processes, decaying with a constant rate that is calculated by using the average carrier density developed under the absorption of the pulse pair. Furthermore, unlike POP or IV scattering, the energy of the scattered carrier is not shifted by a quantum but can fall into a continuum of values, constrained by the conservation of energy and crystal momentum for the scattering particles. Third, theoretical expressions found in the literature concerning these carrier-density-dependent processes almost universally assume a carrier distribution at equilibrium (see, for example, Ref. 21). However, under our experimental conditions, the carrier distribution is highly nonequilibrium- and delta-function-like in character.

Expressions for the free carrier scattering rate as well as for the POP scattering rate involve the screening parameter $q_o$. Under equilibrium conditions, $q_o$ is given by the well-known formula[21]

$$q_o^2 = 4\pi e^2 n/\epsilon k_B T_c, \quad (37)$$

where $T_c$ is the temperature of the carrier system. This expression for $q_o$ was used in our calculations even though its validity under nonequilibrium conditions has not been established. The problem of screening under nonequilibrium conditions clearly needs further consideration.

An expression for POP scattering that includes screening but ignores the valley nonparabolicity is

$$R_{POP}^{+,-} = e\zeta(2mE)^{1/2}\begin{cases} N(\omega_{op}) \\ N(\omega_{op}) + 1 \end{cases} \times \{\tfrac{1}{2}\ln[(q_{max}^2 + q_o^2)/(q_{min}^2 + q_o^2)] + \tfrac{1}{2}q_o^2[(q_{max}^2 + q_o^2)^{-1} + (q_{min}^2 + q_o^2)^{-1}\}, \quad (38)$$

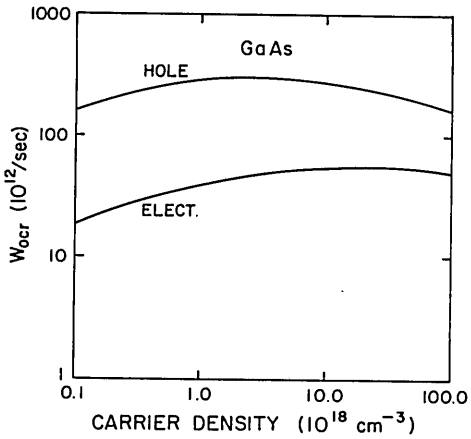


Fig. 7. Calculated free-carrier–carrier rate out of the OCR versus carrier density for GaAs.

where $q_{\max,\min}$ are the limits on the phonon wave vector. For absorption,

$$q_{\max,\min} = k[(1 + \hbar\omega_{op}/E)^{1/2} \pm 1], \tag{39}$$

with $k$ being the initial carrier wave vector. For emission,

$$q_{\max,\min} = k[1 \pm (1 - \hbar\omega_{op}/E)^{1/2}]. \tag{40}$$

At a carrier density of $10^{19}$ cm$^{-3}$, the calculated effect of screening on POP scattering is to reduce this rate by a factor of about 2 from its unscreened value.

Screening also affects the character of carrier–carrier scattering. The differential cross section for a collision between two free identical particles given by Ridley[22] is

$$\begin{aligned}\sigma(\alpha, \mathbf{k}_{cm}) = U\{&\mathbf{k}_{cm}{}^2(1 + \cos\alpha) + q_o{}^2/4]^{-2} \\ &+ [\mathbf{k}_{cm}{}^2(1 - \cos\alpha) + q_0{}^2/4]^{-2} \\ &+ [\mathbf{k}_{cm}{}^2(1 + \cos\alpha) + q_o{}^2/4]^{-1} \\ &\times [\mathbf{k}_{cm}{}^2(1 - \cos\alpha) + q_o{}^2/4]^{-1}\},\end{aligned} \tag{41}$$

where $U = e^4\mu^2/\epsilon^2\hbar^4$, $\mathbf{k}_{cm}$ is the wave vector of the particle in the center-of-mass frame, $\alpha$ is the scattering angle, and $\mu$ is the reduced mass. The expression for unlike-particle collision is just the first term of Eq. (41). The effect of screening on carrier–carrier collisions is to increase the predominance of forward angle scattering for small values of $q_o/\mathbf{k}_{cm}$. As $q_o$ grows, the characteristic scattering angle increases.

In the limit of large $q_o$, when the screening length $1/q_o$ is larger than the intercarrier spacing, collective oscillations of the plasma become the dominant mode of excitation, and two-body collisions are no longer relevant. The collective oscillations carry quanta of energy $\hbar\omega_p$, where $\hbar\omega_p$ is the plasma frequency. We are not aware of an expression for carrier–plasmon scattering applicable to a monoenergetic carrier distribution.

The effect of free carrier scattering on $T_r$ can be estimated by considering a density of monoenergetic carriers having an energy that places them in the OCR but with a random distribution of wave-vector directions. We calculate the rate of scattering events between carriers that remove carriers from the OCR, averaged over all possible pairs of carriers. Whether a scattering event removes a carrier from the OCR depends on the scattered wave-vector direction and magnitude and on the size of the OCR.

We have numerically calculated this rate for an assumed size of the OCR, summing over all possible final states, counting only those outside the OCR, and weighing each by the cross section for that event given by Eq. (41). The rates for electron–hole and electron–electron scattering were summed to give the total rate for electrons, and similarly for holes.

The resulting rate of scattering out of the OCR, denoted $W_{OCR}$, is given in Fig. 7 for electrons and holes in GaAs. The chief result is that $W_{OCR}$ for holes is an order of magnitude larger than that for electrons. This is because $W_{OCR}$ is proportional to the effective mass. The lack of a strong density dependence in the rates is due to the counteractive effects of increased screening and the increased frequency of collisions as the carrier density increases. Calculated $W_{OCR}$ for AlGaAs is similar in its magnitude and density dependence to the results shown in Fig. 7 for GaAs. Although the experimentally measured values for $T_r$ show a density dependence for the AlGaAs sample, but not for the GaAs sample, this calculation of $W_{OCR}$ provides no theoretical reason for the difference in behavior for the two materials.

In the calculation, the resulting value of $W_{OCR}$ at low carrier density is sensitive to the size of the OCR assumed. The value used here, 40 meV for the uncertainty in the transition energy, was based on a semiconductor state lifetime of ~50 fsec, together with the measured bandwidth of the laser light. The calculated result, that $W_{OCR}$ for holes corresponds to a 10-fsec relaxation time, indicates a lack of self-consistency in the calculation of $W_{OCR}$. For if the semiconductor-state lifetime is indeed 10 fsec, as this calculation suggests, then a much broader OCR would result. This in turn would yield a relaxation time for holes much slower than 10 fsec, since more scattered states will fall inside rather than outside the OCR.

This lack of self-consistency indicates that a more comprehensive treatment of the entire problem of carrier–carrier scattering must be found before detailed quantitative comparison between theory and experiment can be made. However, it is likely that the order-of-magnitude faster scattering rate for holes than for electrons would also result from such a calculation. As discussed in Section 4, this result implies that the experimentally measured value for $T_r$ can be attributed to decay of electron distribution rather than to that of hole distribution.

## 6. CONCLUSIONS

In conclusion, we have presented our results on the femtosecond relaxation of hot carriers in GaAs, $Al_{0.32}Ga_{0.68}As$, and a MQW structure in which we have measured relaxation times of carriers from their initially excited states to be in the range of 50–100 fsec. We have described the theoretical foundations of our experimental technique, the equal-pulse correlation technique, with a detailed analysis of the CA. This is the first reported analysis of the CA contribution in the geometry of parallel copropagating beams and the first reported calculation of the saturable-absorption symmetry coefficients for GaAs and related materials. We have described the interpretation of the measured relaxation time in terms of the decay of electron and hole response functions and concluded that it corresponds mainly to the decay of electron population. Relevant carrier-density-independent scattering processes have been described and their corresponding rates calculated. The IV phonon-scattering process is found to be the dominant

scattering process. Using these calculated scattering rates and the electron response only to determine the relaxation time yielded relaxation times of 30 fsec in GaAs and 40 fsec in AlGaAs in this low-carrier-density limit, in reasonable agreement with our data. Carrier-density-dependent processes have been discussed, and the corresponding rates are estimated wherever possible. The carrier-density dependence of our data is, however, not yet completely understood.

## ACKNOWLEDGMENTS

We thank V. Kreismanis for sample growth and preparation. This research was supported by the National Science Foundation through the Materials Science Center of Cornell University and by the Joint Services Electronics Program.

* Permanent address, AT&T Bell Laboratories, Crawford Hill Laboratory, Holmdel, New Jersey 07733.

† Permanent address, Department of Physics, University of California, Berkeley, California 94720.

## REFERENCES

1. J. L. Oudar, A. Migus, D. Hulin, G. Grillon, J. Etchepare, and A. Antonetti, Phys. Rev. Lett. **53,** 384 (1984).
2. C. Shank, R. Fork, R. Yen, J. Shah, B. Greene, A. Gossard, and C. Weisbuch, Solid State Commun. **47,** 981 (1983).
3. R. Seymour, M. Junnarkar, and R. Alfano, Solid State Commun. **41,** 657 (1982).
4. D. von der Linde and R. Lambrich, Phys. Rev. Lett. **42,** 1090 (1979).
5. A. Smirl, J. Lindle, and S. Moss, Phys. Rev. B **18,** 5489 (1978).
6. C. L. Tang and D. J. Erskine, Phys. Rev. Lett. **51,** 840 (1983).
7. D. J. Erskine, A. J. Taylor, and C. L. Tang, Appl. Phys. Lett. **45,** 54 (1984).
8. A. J. Taylor, D. J. Erskine, and C. L. Tang, in *Proceedings of the IVth Workshop on Ultrafast Phenomena* (Springer-Verlag, Berlin, 1984).
9. A. J. Taylor, D. J. Erskine, and C. L. Tang, Appl. Phys. Lett. **43,** 989 (1983).
10. E. P. Ippen and C. V. Shank, "Techniques for measurement," in *Ultrashort Light Pulses*, S. Shapiro, ed. (Springer-Verlag, New York, 1977).
11. J. Blakemore, J. Appl. Phys. **53,** R123 (1982).
12. B. S. Wherrett, A. L. Smirl, and T. F. Bogess, IEEE J. Quantum Electron. **QE-19,** 680 (1983).
13. N. Bloembergen, *Nonlinear Optics* (Benjamin, Reading, Mass., 1965).
14. T. F. Heinz, S. L. Palfrey, and K. B. Eisenthal, Opt. Lett. **9,** 359 (1984).
15. E. O. Kane, J. Phys. Chem. Solids **1,** 249 (1957).
16. A. R. Edmonds, *Angular Momentum in Quantum Mechanics* (Princeton U. Press, Princeton, N.J., 1957).
17. W. Fawcett, A. Boardman, and S. Swain, J. Phys. Chem. Solids **31,** 1963 (1970).
18. J. Hauser, M. Littlejohn, and T. Glisson, Appl. Phys. Lett. **28,** 459 (1976).
19. M. Littlejohn, J. Hauser, T. Glisson, D. Ferry, and J. Harrison, Solid State Electron. **21,** 107 (1978).
20. M. Littlejohn, J. Hauser, and T. Glisson, J. Appl. Phys. **48,** 4587 (1977).
21. D. Pines and D. Bohm, Phys. Rev. **85,** 338 (1952).
22. B. Ridley, *Quantum Processes in Semiconductors* (Clarendon, Oxford, 1979).